Free Vibration Analysis of Laminated Composite Plates based on FSDT using One-Dimensional IRBFN Method

D. Ngo-Cong[a,b], N. Mai-Duy[a], W. Karunasena[b], T. Tran-Cong[a,*]

[a] *Computational Engineering and Science Research Centre, Faculty of Engineering and Surveying, The University of Southern Queensland, Toowoomba, QLD 4350, Australia*
[b] *Centre of Excellence in Engineered Fibre Composites, Faculty of Engineering and Surveying, The University of Southern Queensland, Toowoomba, QLD 4350, Australia*

Abstract

This paper presents a new effective radial basis function (RBF) collocation technique for the free vibration analysis of laminated composite plates using the first order shear deformation theory (FSDT). The plates, which can be rectangular or non-rectangular, are simply discretised by means of Cartesian grids. Instead of using conventional differentiated RBF networks, one-dimensional integrated RBF networks (1D-IRBFN) are employed on grid lines to approximate the field variables. A number of examples concerning various thickness-to-span ratios, material properties and boundary conditions are considered. Results obtained are compared with the exact solutions and numerical results by other techniques in the literature to investigate the performance of the proposed method.

Keywords: laminated composite plates; free vibration; rectangular and non-rectangular domains; integrated radial basis functions; Cartesian grids.

1. Introduction

Free vibration analysis of laminated composite plates has been an important problem in the design of mechanical, civil and aerospace applications. Vibration can waste energy and create unwanted noise in the motions of engines, motors, or any mechanical devices in operation. When a system operates at the system natural frequency, resonance can happen causing large

*Correspondence author: Tel: +61 7 4631-1332/-2539, Fax: +61 7 46312526.
Email address: trancong@usq.edu.au (T. Tran-Cong)

deformations and even catastrophic failure in improperly constructed structures. Careful designs can minimize those unwanted vibrations.

The lamination scheme and material properties of individual lamina provide an added flexibility to designers to tailor the stiffness and strength of composite laminates to match the structural requirements. The significant difference between the classical plate theory (CLPT) and the first order shear deformation theory (FSDT) is the effect of including transverse shear deformation on the predicted deflections and frequencies. The CLPT underpredicts deflections and overpredicts frequencies for plates with thickness-to-length ratios larger than 0.05 [1] while the FSDT has been the most commonly used in the vibration analysis of moderately thick composite plates with thickness-to-length ratio less than 0.2 [2]. The FSDT is an approximate theory with some assumptions on the deformation of a plate which reduce the dimensions of the plate problem from three to two and greatly simplify the governing equations. However, these assumptions inherently result in errors which can be significant when the thickness-to-length ratio increases.

Using the theory of elasticity, Srinivas et al. [3] developed an exact three-dimensional solution for bending, vibration and buckling of simply supported thick orthotropic rectangular plates. Their results have been widely used as benchmark solutions by many researchers. Liew et al. [4] developed a continuum three-dimensional Ritz formulation based on the three-dimensional elasticity theory and the Ritz minimum energy principle for the vibration analysis of homogeneous, thick, rectangular plates with arbitrary combination of boundary constraints. The formulation was employed to study the effects of geometric parameters on the overall normal mode characteristics of simply supported plates, and the effects of in-plane inertia on the vibration frequencies of plates with different thicknesses [5]. This formulation was also applied specifically to investigate the effects of boundary constraints and thickness ratios on the vibration responses of these plates [6]. Liew and Teo [7] employed the differential quadrature (DQ) method for the vibration analysis of three-dimensional elasticity plates with a high degree of accuracy.

When dealing with highly orthotropic composite plates, the higher-order shear deformation theories (HSDT) is more favourable than the FSDT because the former can yield highly accurate results without the need for a shear correction factor. Reddy and Phan [8] employed the HSDT [9] to determine the natural frequencies and buckling loads of elastic plates. Their exact solutions obtained were more accurate than those of the FSDT and CLPT when compared with the exact solutions by three-dimensional elastic-

ity theory. Lim et al. [10, 11] developed an energy-based higher-order plate theory in association with geometrically oriented shape function to investigate the free vibration of thick shear deformable, rectangular plates with arbitrary combinations of boundary constraints. This method required considerably less memory than the direct three-dimensional elasticity analysis while maintaining the same level of accuracy. Their numerical results showed that for transverse-dominant vibration modes, an increase in thickness results in higher frequency while for inplane-dominant vibration modes, the effects of variation in thickness is insignificant.

It is highly desirable to develop an efficient numerical method to investigate and optimize the characteristic properties of laminated plates instead of using experimental testing due to time and cost efficiencies. Because of the limitations of analytical methods in practical applications, numerical methods are becoming the most effective tools to solve many industrial problems. Finite element method (FEM) is a powerful method used to solve most linear and nonlinear practical engineering problems in solid and fluid mechanics. However, FEM has some limitations which include time-consuming task of mesh generation, low accuracy in stress calculation, low accuracy when solving large deformation problems due to element distortions, difficulty in simulating problems with strain localization and shear band formation due to discontinuities that may not coincide with some of the original nodal lines [12]. Meshless method has great potential to overcome those challenges.

There have been a number of meshless methods developed in the past years. Nayroles el al. [13] introduced the diffuse element method (DEM), a first meshless method using moving least square (MLS) approximations to construct the shape function. The finite element mesh is totally unnecessary in this method. Belytschko et al. [14] proposed an element-free Galerkin (EFG) method based on the DEM with modifications in the implementation to increase the accuracy and the rate of convergence. In their work, the Lagrange multipliers were used to impose essential boundary conditions. Atluri and Zhu [15] presented a meshless local Petrov-Galerkin (MLPG) approach based on a local symmetric weak form and the MLS approximation, which is a truly meshless method. The essential boundary conditions in their formulation were enforced by a penalty method. Liu and Gu [16] developed a point interpolation method (PIM) to construct polynomial interpolation functions with delta function property so the essential boundary conditions can be imposed as done in the conventional FEM with ease. However, the problem of singular moment matrix can occur, resulting in termination of

the computation. A point interpolation method based on RBF (RPIM) was proposed by Wang and Liu [17] to produce a non-singular moment matrix. Liew et al. [18, 19] proposed a numerical algorithm based on the RPIM for the buckling analysis of rectangular, circular, trapezoidal and skew Mindlin plates that are subjected to non-uniformly distributed in-plane edge loads. In the PIM and RPIM, the compatibility characteristic is not ensured so the field function approximated could be discontinuous when nodes enter or leave the moving support domain. Liu et al. suggested a linearly conforming point interpolation method (RC-PIM) [20] with a simple scheme for local supporting node selection, and a linearly conforming radial point interpolation method (RC RPIM) [21] to overcome the singular moment matrix issue and ensure the compatibility of the displacement.

In 1990, Kansa proposed a collocation scheme based on multiquadric (MQ) radial basis functions for the numerical solution of partial differential equations (PDEs) [22, 23]. Their numerical results showed that MQ scheme yielded an excellent interpolation and partial derivative estimates for a variety of two-dimensional functions over both gridded and scattered data. The main drawback of RBF based methods is the lack of mathematical theories for finding the appropriate values of network parameters. For example, the RBF width, which strongly affects the performance of RBF networks, has still been chosen either by empirical approaches or by optimization techniques. The use of RBF based method for the free vibration analysis of laminated composite plates has been previously studied by numerous authors. The MQ-RBF procedure was used to predict the free vibration behaviour of moderately thick symmetrically laminated composite plates by Ferreira et al. [24]. The free vibration analysis of Timoshenko beams and Mindlin plates using Kansa's non-symmetric RBF collocation method was performed by Ferreira and Fasshauer [25]. Ferreira and Fasshauer [26] showed that the combination of RBF and pseudospectral methods produces highly accurate results for free vibration analysis of symmetric composite plates. Liew [27] proposed a p-Ritz method with high accuracy, but, it is difficult to choose the appropriate trial functions for complicated problems. Karunasena et al. [28, 29] investigated natural frequencies of thick arbitrary quadrilateral plates and shear-deformable general triangular plates with arbitrary combinations of boundary conditions using the pb-2 Rayleigh-Ritz method in conjunction with the FSDT. Liew et al. [30] proposed the harmonic reproducing kernel particle method for the free vibration analysis of rotating cylindrical shells. This technique provides ease of enforcing vari-

ous types of boundary conditions and concurrently is able to capture the travelling modes. Zhao et al. [31] employed the reproducing kernel particle estimation in hybridized form with harmonic functions to study the frequency characteristics of cylindrical panels. Liew et al. [32] presented a meshfree kernel particle Ritz method (kp-Ritz) for the geometrically nonlinear analysis of laminated composite plates with large deformations, which is based on the FSDT and the total Lagrangian formulation. Liew et al. [33] adopted a moving least squares differential quadrature (MLSDQ) method for predicting the free vibration behaviour of square, circular and skew plates with various boundary conditions. A meshfree method based on the reproducing kernel particle approximate for the free vibration and buckling analyses of shear-deformation plates was conducted by Liew [34]. In this method, the essential boundary conditions were enforced by a transformation technique.

As an alternative to the conventional differentiated radial basis function networks (DRBFN) method, Mai-Duy and Tran-Cong [35] proposed the use of integration to construct the RBFN expressions (the IRBFN method) for the approximation of a function and its derivatives and for the solution of PDEs. The use of integration instead of conventional differentiation to construct the RBF approximations significantly improved the stability and accuracy of the numerical solution. The improvement is attributable to the fact that integration is a smoothing operation and is more numerically stable. The numerical results showed that the IRBFN method achieves superior accuracy [35, 36]. Mai-Duy and Tran-Cong [37] presented a mesh-free IRBFN method using Thin Plate Splines (TPSs) for numerical solution of differential equations (DEs) in rectangular and curvilinear coordinates. The IRBFN was also used to simulate the static analysis of moderately-thick laminated composite plates using the FSDT [38].

A one-dimensional integrated radial basis function networks (1D-IRBFN) collocation method for the solution of second- and fourth-order PDEs was presented by Mai-Duy and Tanner [39]. Along grid lines, 1D-IRBFN are constructed to satisfy the governing DEs together with boundary conditions in an exact manner. The 1D-IRBFN method was further developed for the simulation of fluid flow problems. In the present study, the 1D-IRBFN method is extended to the case of free vibration of composite laminates based on FSDT. A number of examples are considered to investigate the effects of various plate shapes, length-to-width ratios, thickness-to-span ratios, material properties and boundary conditions on natural frequencies of composite laminated plates. The results obtained are compared with available published

results from different methods.

The paper is organised as follows. Section 2 describes the governing equations based on FSDT and boundary conditions for the free vibration of laminated composite plates. The 1D-IRBFN-based Cartesian-grid technique is presented in Section 3. The discretisation of the governing equations and boundary conditions is described in Section 4. The proposed technique is then validated through several test examples in Section 5. Section 6 concludes the paper.

2. Governing equations

2.1. First-order shear deformation theory

In the FSDT [1], the transverse normals do not remain perpendicular to the midsurface after deformation due to the effects of transverse shear strains. The inextensibility of transverse normals requires w not to be a function of the thickness coordinate z. The displacement field of the FSDT at time t is of the form

$$u(x, y, z, t) = u_0(x, y, t) + z\phi_x(x, y, t), \tag{1}$$

$$v(x, y, z, t) = v_0(x, y, t) + z\phi_y(x, y, t), \tag{2}$$

$$w(x, y, z, t) = w_0(x, y, t), \tag{3}$$

where (u_0, v_0, w_0) denotes the vector of displacement of a point on the plane $z = 0$, and ϕ_x and ϕ_y are, respectively, the rotations of a transverse normal about the $y-$ and $x-$ axes.

Since the transverse shear strains are assumed to be constant through the laminate thickness, it follows that the transverse shear stresses will also be constant. However, in practice, the transverse shear stresses vary at least quadratically through layer thickness. This discrepancy between the actual stress state and the constant stress state predicted by the FSDT is often corrected by a parameter K_s, called the shear correction coefficient. It is noted that the natural frequencies of the plate are affected by the factor K_s and the rotary inertia (RI). The smaller the values of K_s and RI, the smaller the frequencies will be.

In this paper we consider a symmetrically laminated plate with the coordinate system origined at the midplane of the laminate, where each layer of the laminate is orthotropic with respect to the $x-$ and $y-$ axes and all layers are of equal thickness. For symmetric laminates, the displacements

u_0 and v_0 can be disregarded due to the uncoupling between extension and bending actions. The equations of motion for the free vibration of symmetric cross-ply laminated plates can be expressed by the dynamic version of the principle of virtual displacements as

$$K_s A_{55}\left(\frac{\partial^2 w}{\partial x^2}+\frac{\partial \phi_x}{\partial x}\right)+K_s A_{44}\left(\frac{\partial^2 w}{\partial y^2}+\frac{\partial \phi_y}{\partial y}\right)=I_0\frac{\partial^2 w}{\partial t^2}, \tag{4}$$

$$D_{11}\frac{\partial^2 w}{\partial x^2}+D_{12}\frac{\partial^2 \phi_y}{\partial x \partial y}+D_{66}\left(\frac{\partial^2 \phi_x}{\partial y^2}+\frac{\partial^2 \phi_y}{\partial x \partial y}\right)-K_s A_{55}\left(\frac{\partial w}{\partial x}+\phi_x\right)=I_2\frac{\partial^2 \phi_x}{\partial t^2}, \tag{5}$$

$$D_{66}\left(\frac{\partial^2 \phi_x}{\partial x \partial y}+\frac{\partial^2 \phi_y}{\partial x^2}\right)+D_{12}\frac{\partial^2 \phi_x}{\partial y^2}+D_{22}\frac{\partial^2 \phi_y}{\partial y^2}-K_s A_{44}\left(\frac{\partial w}{\partial y}+\phi_y\right)=I_2\frac{\partial^2 \phi_y}{\partial t^2}, \tag{6}$$

where I_0 and I_2 are the mass inertia tensor components defined as

$$I_0=\rho h, \tag{7}$$

$$I_2=\frac{\rho h^3}{12}, \tag{8}$$

in which ρ and h denote the density and the total thickness of the composite plate, respectively; and A_{ij} and D_{ij} are the extensional and bending stiffnesses given by

$$A_{ij}=\sum_{k=1}^{N}\bar{Q}_{ij}^{(k)}(z_{k+1}-z_k), \tag{9}$$

$$D_{ij}=\frac{1}{3}\sum_{k=1}^{N}\bar{Q}_{ij}^{(k)}(z_{k+1}^3-z_k^3), \tag{10}$$

in which $\bar{Q}_{ij}^{(k)}$ is the transformed material plane stress-reduced stiffness matrix of the layer k.

In (9) and (10), the matrix $\bar{Q}_{ij}^{(k)}$ can be obtained through

$$\bar{\mathbf{Q}}=\mathbf{T}\mathbf{Q}_m\mathbf{T}^T, \tag{11}$$

where $\mathbf{T}$ is the transformation matrix given by

$$\mathbf{T} = \begin{bmatrix} \cos^2\theta & \sin^2\theta & 0 & 0 & -\sin 2\theta \\ \sin^2\theta & \cos^2\theta & 0 & 0 & \sin 2\theta \\ 0 & 0 & \cos\theta & \sin\theta & 0 \\ 0 & 0 & -\sin\theta & \cos\theta & 0 \\ \sin\theta\cos\theta & -\sin\theta\cos\theta & 0 & 0 & \cos^2\theta - \sin^2\theta \end{bmatrix}, \quad (12)$$

and $\mathbf{Q}_m$ is the material plane stress-reduced stiffness

$$\mathbf{Q}_m = \begin{bmatrix} E_1/(1-\nu_{12}.\nu_{21}) & \nu_{12}.E_2/(1-\nu_{12}.\nu_{21}) & 0 & 0 & 0 \\ \nu_{12}.E_2/(1-\nu_{12}.\nu_{21}) & E_2/(1-\nu_{12}.\nu_{21}) & 0 & 0 & 0 \\ 0 & 0 & G_{23} & 0 & 0 \\ 0 & 0 & 0 & G_{13} & 0 \\ 0 & 0 & 0 & 0 & G_{12} \end{bmatrix}, \quad (13)$$

in which E_1 and E_2 are the Young's moduli for a layer parallel to fibres and perpendicular to fibres, respectively, ν_{12} and ν_{21} are Poisson's ratios, and G_{23}, G_{13}, and G_{12} are shear moduli in the $2-3, 1-3$, and $1-2$ planes, respectively.

Expressing the variables w, ϕ_x, and ϕ_y in the following harmonic forms

$$w(x,y,t) = W(x,y)e^{i\omega t}, \quad (14)$$

$$\phi_x(x,y,t) = \Psi_x(x,y)e^{i\omega t}, \quad (15)$$

$$\phi_y(x,y,t) = \Psi_y(x,y)e^{i\omega t}, \quad (16)$$

the equations of motion (4), (5) and (6) become

$$K_s A_{55}\left(\frac{\partial^2 w}{\partial x^2} + \frac{\partial \Psi_x}{\partial x}\right) + K_s A_{44}\left(\frac{\partial^2 w}{\partial y^2} + \frac{\partial \Psi_y}{\partial y}\right) = -I_0\omega^2 W, \quad (17)$$

$$D_{11}\frac{\partial^2 w}{\partial x^2} + D_{12}\frac{\partial^2 \Psi_y}{\partial x \partial y} + D_{66}\left(\frac{\partial^2 \Psi_x}{\partial y^2} + \frac{\partial^2 \Psi_y}{\partial x \partial y}\right) - K_s A_{55}\left(\frac{\partial w}{\partial x} + \Psi_x\right) = -I_2\omega^2\Psi_x, \quad (18)$$

$$D_{66}\left(\frac{\partial^2 \Psi_x}{\partial x \partial y} + \frac{\partial^2 \Psi_y}{\partial x^2}\right) + D_{12}\frac{\partial^2 \Psi_x}{\partial y^2} + D_{22}\frac{\partial^2 \Psi_y}{\partial y^2} - K_s A_{44}\left(\frac{\partial w}{\partial y} + \Psi_y\right) = -I_2\omega^2\Psi_y, \quad (19)$$

where ω is the frequency of natural vibration.

2.2. Boundary conditions

The boundary conditions for a simply supported or clamped edge can be described as follows.

- Simply supported case: There are two kinds of simply support boundary conditions for the FSDT plate models.
  - The first kind is the soft simple support (SS1)

$$w = 0;\ M_{ns} = 0;\ M_n = 0. \tag{20}$$

  - The second kind is the hard simple support (SS2)

$$w = 0;\ \phi_s = 0;\ M_n = 0. \tag{21}$$

  The hard simple support is considered in this paper. From (21), we have the following relations

$$w = 0, \qquad \text{on } \Gamma, \tag{22}$$
$$n_x\phi_y - n_y\phi_x = 0, \qquad \text{on } \Gamma, \tag{23}$$
$$n_x^2 M_{xx} + 2n_x n_y M_{xy} + n_y^2 M_y = 0, \qquad \text{on } \Gamma, \tag{24}$$

  in which n_x and n_y are the direction cosines of a unit normal vector at a point on the plate boundary Γ.

  Equations (24) can be expressed as

$$\left(n_x^2 D_{11} + n_y^2 D_{12}\right)\frac{\partial \phi_x}{\partial x} + 2n_x n_y D_{66}\left(\frac{\partial \phi_x}{\partial y} + \frac{\partial \phi_y}{\partial x}\right) + \left(n_x^2 D_{12} + n_y^2 D_{22}\right)\frac{\partial \phi_y}{\partial y} = 0. \tag{25}$$

- Clamped case:

$$w = 0;\ \phi_n = 0;\ \phi_s = 0. \tag{26}$$

  Clamped boundary conditions (26) can be described as follows.

$$w = 0, \qquad \text{on } \Gamma, \tag{27}$$
$$\phi_x = 0, \qquad \text{on } \Gamma, \tag{28}$$
$$\phi_y = 0, \qquad \text{on } \Gamma. \tag{29}$$

In (20), (21) and (26), the subscripts n and s represent the normal and tangential directions of the edge, respectively; M_n and M_{ns} denotes the normal bending moment and twisting moment, respectively; and ϕ_n and ϕ_s are rotations about the tangential and normal coordinates on the laminate edge.

3. One-dimensional indirect/integrated radial basis function networks

In the remainder of the article, we use

- the notation $\widehat{[\,]}$ for a vector/matrix $[\,]$ that is associated with a grid line,
- the notation $\widetilde{[\,]}$ for a vector/matrix $[\,]$ that is associated with the whole set of grid lines,
- the notation $[\,]_{(\eta,\theta)}$ to denote selected rows η and columns θ of the matrix $[\,]$,
- the notation $[\,]_{(\eta)}$ to pick out selected components η of the vector $[\,]$,
- the notation $[\,]_{(:,\theta)}$ to denote all rows and pick out selected columns θ of the matrix $[\,]$, and
- the notation $[\,]_{(\eta,:)}$ to denote all columns and pick out selected rows η of the matrix $[\,]$.

The domain of interest is discretised using a Cartesian grid, i.e. an array of straight lines that run parallel to the $x-$ and $y-$ axes. The dependent variable u and its derivatives on each grid line are approximated using an IRBF interpolation scheme as described in the remainder of this section.

3.1. IRBFN expressions on a grid line (1D-IRBF scheme)

Consider an $x-$ grid line, e.g. $[j]$, as shown in Fig. 1. The variation of u along this line is sought in the IRBF form. The second-order derivative of u is decomposed into RBFs; the RBF network is then integrated once and twice to obtain the expressions for the first-order derivative of u and the solution u itself,

$$\frac{\partial^2 u(x)}{\partial x^2} = \sum_{i=1}^{N_x^{[j]}} w^{(i)} g^{(i)}(x) = \sum_{i=1}^{N_x^{[j]}} w^{(i)} H_{[2]}^{(i)}(x), \tag{30}$$

$$\frac{\partial u(x)}{\partial x} = \sum_{i=1}^{N_x^{[j]}} w^{(i)} H_{[1]}^{(i)}(x) + c_1, \tag{31}$$

$$u(x) = \sum_{i=1}^{N_x^{[j]}} w^{(i)} H_{[0]}^{(i)}(x) + c_1 x + c_2, \tag{32}$$

where $N_x^{[j]}$ is the number of nodes on the grid line $[j]$; $\{w^{(i)}\}_{i=1}^{N_x^{[j]}}$ are RBF weights to be determined; $\left\{g^{(i)}(x)\right\}_{i=1}^{N_x^{[j]}} = \left\{H_{[2]}^{(i)}(x)\right\}_{i=1}^{N_x^{[j]}}$ are known RBFs, e.g., for the case of multiquadrics $g^{(i)}(x) = \sqrt{(x-x^{(i)})^2 + a^{(i)2}}$, $a^{(i)}$ - the RBF width; $H_{[1]}^{(i)}(x) = \int H_{[2]}^{(i)}(x)dx$; $H_{[0]}^{(i)}(x) = \int H_{[1]}^{(i)}(x)dx$; and c_1 and c_2 are integration constants which are also unknown.

It is more convenient to work in the physical space than in the network-weight space. The RBF coefficients including two integration constants can be transformed into the meaningful nodal variable values through the following relation

$$\hat{u} = \hat{\mathbf{H}} \begin{pmatrix} \hat{w} \\ \hat{c} \end{pmatrix}, \tag{33}$$

where $\hat{\mathbf{H}}$ is an $N_x^{[j]} \times (N_x^{[j]} + 2)$ matrix whose entries are $\hat{H}_{ij} = H_{[0]}^{[j]}(x^{(i)})$, $\hat{u} = (u^{(1)}, u^{(2)}, ..., u^{(N_x^{[j]})})^T$, $\hat{w} = (w^{(1)}, w^{(2)}, ..., w^{(N_x^{[j]})})^T$ and $\hat{c} = (c_1, c_2)^T$. There are two possible transformation cases.

Non-square conversion matrix (NSCM): The direct use of (33) leads to an underdetermined system of equations

$$\hat{u} = \hat{\mathbf{H}} \begin{pmatrix} \hat{w} \\ \hat{c} \end{pmatrix} = \hat{\mathbf{C}} \begin{pmatrix} \hat{w} \\ \hat{c} \end{pmatrix}, \tag{34}$$

or

$$\begin{pmatrix} \hat{w} \\ \hat{c} \end{pmatrix} = \hat{\mathbf{C}}^{-1} \hat{u}, \tag{35}$$

where $\hat{\mathbf{C}} = \hat{\mathbf{H}}$ is the conversion matrix whose inverse can be found using the SVD technique.

Square conversion matrix (SCM): Due to the presence of c_1 and c_2, one can add two additional equations of the form

$$\hat{f} = \hat{\mathbf{K}} \begin{pmatrix} \hat{w} \\ \hat{c} \end{pmatrix} \tag{36}$$

to equation system (34). For example, in the case of Neumann boundary

conditions, this subsystem can be used to impose derivative boundary values

$$\hat{f} = \begin{pmatrix} \frac{\partial u}{\partial x}(x^{(1)}) \\ \frac{\partial u}{\partial x}(x^{(N_x^{[j]})}) \end{pmatrix}, \tag{37}$$

$$\hat{\mathbf{K}} = \begin{bmatrix} H_{[1]}^{(1)}(x^{(1)}) & H_{[1]}^{(2)}(x^{(1)}) & ... & H_{[1]}^{(N_x^{[j]})}(x^{(1)}) & 1 & 0 \\ H_{[1]}^{(1)}(x^{(N_x^{[j]})}) & H_{[1]}^{(2)}(x^{(N_x^{[j]})}) & ... & H_{[1]}^{(N_x^{[j]})}(x^{(N_x^{[j]})}) & 1 & 0 \end{bmatrix}. \tag{38}$$

The conversion system can be written as

$$\begin{pmatrix} \hat{u} \\ \hat{f} \end{pmatrix} = \begin{bmatrix} \hat{\mathbf{H}} \\ \hat{\mathbf{K}} \end{bmatrix} \begin{pmatrix} \hat{w} \\ \hat{c} \end{pmatrix} = \hat{\mathbf{C}} \begin{pmatrix} \hat{w} \\ \hat{c} \end{pmatrix}, \tag{39}$$

or

$$\begin{pmatrix} \hat{w} \\ \hat{c} \end{pmatrix} = \hat{\mathbf{C}}^{-1} \begin{pmatrix} \hat{u} \\ \hat{f} \end{pmatrix}. \tag{40}$$

It can be seen that (35) is a special case of (40), where $\hat{f}$ is simply set to null. By substituting equation (40) into equations (30) and (31), the second- and first-order derivatives of the variable u are expressed in terms of nodal variable values

$$\frac{\partial^2 u(x)}{\partial x^2} = \left(H_{[2]}^{(1)}(x), H_{[2]}^{(2)}(x), ..., H_{[2]}^{(N_x^{[j]})}(x), 0, 0 \right) \hat{\mathbf{C}}^{-1} \begin{pmatrix} \hat{u} \\ \hat{f} \end{pmatrix}, \tag{41}$$

$$\frac{\partial u(x)}{\partial x} = \left(H_{[1]}^{(1)}(x), H_{[1]}^{(2)}(x), ..., H_{[1]}^{(N_x^{[j]})}(x), 1, 0 \right) \hat{\mathbf{C}}^{-1} \begin{pmatrix} \hat{u} \\ \hat{f} \end{pmatrix}, \tag{42}$$

or

$$\frac{\partial^2 u(x)}{\partial x^2} = \bar{D}_{2x} \hat{u} + k_{2x}(x), \tag{43}$$

$$\frac{\partial u(x)}{\partial x} = \bar{D}_{1x} \hat{u} + k_{1x}(x), \tag{44}$$

where k_{1x} and k_{2x} are scalars whose values depend on x, f_1 and f_2; and $\bar{D}_{1x}$ and $\bar{D}_{2x}$ are known vectors of length $N_x^{[j]}$.

Application of equation (43) and (44) to boundary and interior points on the grid line $[j]$ yields

$$\widehat{\frac{\partial^2 u^{[j]}}{\partial x^2}} = \hat{\mathbf{D}}_{2x}^{[j]} \hat{u} + \hat{k}_{2x}^{[j]}, \tag{45}$$

$$\widehat{\frac{\partial u^{[j]}}{\partial x}} = \hat{\mathbf{D}}_{1x}^{[j]} \hat{u} + \hat{k}_{1x}^{[j]}, \tag{46}$$

where $\hat{\mathbf{D}}_{1x}^{[j]}$ and $\hat{\mathbf{D}}_{2x}^{[j]}$ are known matrices of dimension $N_x^{[j]} \times N_x^{[j]}$ and $\hat{k}_{1x}^{[j]}$ and $\hat{k}_{2x}^{[j]}$ are known vectors of length $N_x^{[j]}$.

Similarly, along a vertical line $[j]$ parallel to the $y-$ axis, the values of the second- and first-order derivatives of u with respect to y at the nodal points can be given by

$$\widehat{\frac{\partial^2 u^{[j]}}{\partial y^2}} = \hat{\mathbf{D}}_{2y}^{[j]} \hat{u} + \hat{k}_{2y}^{[j]}, \tag{47}$$

$$\widehat{\frac{\partial u^{[j]}}{\partial y}} = \hat{\mathbf{D}}_{1y}^{[j]} \hat{u} + \hat{k}_{1y}^{[j]}. \tag{48}$$

3.2. 1D-IRBFN expressions over the whole computational domain

The values of the second- and first-order derivatives of u with respect to x at the nodal points over the problem domain can be given by

$$\widetilde{\frac{\partial^2 u}{\partial x^2}} = \tilde{\mathbf{D}}_{2x} \tilde{u} + \tilde{k}_{2x}, \tag{49}$$

$$\widetilde{\frac{\partial u}{\partial x}} = \tilde{\mathbf{D}}_{1x} \tilde{u} + \tilde{k}_{1x}, \tag{50}$$

where

$$\tilde{u} = \left(u^{(1)}, u^{(2)}, ..., u^{(N)}\right)^T, \tag{51}$$

$$\widetilde{\frac{\partial^2 u}{\partial x^2}} = \left(\frac{\partial^2 u^{(1)}}{\partial x^2}, \frac{\partial^2 u^{(2)}}{\partial x^2}, ..., \frac{\partial^2 u^{(N)}}{\partial x^2}\right)^T, \tag{52}$$

$$\widetilde{\frac{\partial u}{\partial x}} = \left(\frac{\partial u^{(1)}}{\partial x}, \frac{\partial u^{(2)}}{\partial x}, ..., \frac{\partial u^{(N)}}{\partial x}\right)^T; \tag{53}$$

and $\tilde{\mathbf{D}}_{1x}$ and $\tilde{\mathbf{D}}_{2x}$ are known matrices of dimension $N \times N$; $\tilde{k}_{1x}$ and $\tilde{k}_{2x}$ are known vectors of length N; and N is the total number of nodal points. The matrices $\tilde{\mathbf{D}}_{1x}$ and $\tilde{\mathbf{D}}_{2x}$ and the vectors $\tilde{k}_{1x}$ and $\tilde{k}_{2x}$ are formed as follows.

$$\tilde{\mathbf{D}}_{2x(idj,idj)} = \hat{\mathbf{D}}_{2x}^{[j]}, \tag{54}$$

$$\tilde{\mathbf{D}}_{1x(idj,idj)} = \hat{\mathbf{D}}_{1x}^{[j]}, \tag{55}$$

$$\tilde{k}_{2x(idj)} = \hat{k}_{2x}^{[j]}, \tag{56}$$

$$\tilde{k}_{1x(idj)} = \hat{k}_{1x}^{[j]}, \tag{57}$$

where idj is the index vector indicating the location of nodes on the $[j]$ grid line over the whole grid.

Similarly, the values of the second- and first-order derivatives of u with respect to y at the nodal points over the problem domain can be given by

$$\widetilde{\frac{\partial^2 u}{\partial y^2}} = \tilde{\mathbf{D}}_{2y}\tilde{u} + \tilde{k}_{2y}, \tag{58}$$

$$\widetilde{\frac{\partial u}{\partial y}} = \tilde{\mathbf{D}}_{1y}\tilde{u} + \tilde{k}_{1y}. \tag{59}$$

The mixed partial derivative of $\tilde{u}$ can be given by

$$\frac{\partial^2 \tilde{u}}{\partial x \partial y} = \frac{1}{2}\left(\tilde{\mathbf{D}}_{1x}\tilde{\mathbf{D}}_{1y} + \tilde{\mathbf{D}}_{1y}\tilde{\mathbf{D}}_{1x}\right)\tilde{u} + \tilde{k}_{2xy} = \tilde{\mathbf{D}}_{2xy}\tilde{u} + \tilde{k}_{2xy}, \tag{60}$$

where $\tilde{k}_{2xy}$ is a known vector of length N.

In the special case of a rectangular domain and NSCM, the nodal values of the derivatives of u over the whole domain can be simply computed by means of Kronecker tensor products as follows.

$$\widetilde{\frac{\partial^2 u}{\partial x^2}} = \left(\hat{\mathbf{D}}_{2x}^{[j]} \otimes \mathbf{I}_y\right)\hat{u} = \tilde{\mathbf{D}}_{2x}\hat{u}, \tag{61}$$

$$\widetilde{\frac{\partial u}{\partial x}} = \left(\mathbf{D}_{1x}^{[j]} \otimes \mathbf{I}_y\right)\hat{u} = \tilde{\mathbf{D}}_{1x}\hat{u}, \tag{62}$$

$$\widetilde{\frac{\partial^2 u}{\partial y^2}} = \left(\mathbf{D}_{2y}^{[j]} \otimes \mathbf{I}_x\right)\hat{u} = \tilde{\mathbf{D}}_{2y}\hat{u}, \tag{63}$$

$$\widetilde{\frac{\partial u}{\partial y}} = \left(\mathbf{D}_{2y}^{[j]} \otimes \mathbf{I}_x\right)\hat{u} = \tilde{\mathbf{D}}_{1y}\hat{u}, \tag{64}$$

where $\mathbf{I}_x$ and $\mathbf{I}_y$ are the identity matrices of dimension $N_x \times N_x$ and $N_y \times N_y$, respectively; $\tilde{\mathbf{D}}_{2x}$, $\tilde{\mathbf{D}}_{1x}$, $\tilde{\mathbf{D}}_{2y}$ and $\tilde{\mathbf{D}}_{1y}$ are known matrices of dimension $N_xN_y \times N_xN_y$; $\tilde{u} = \left(u^{(1)}, u^{(2)}, ..., u^{(N_xN_y)}\right)^T$; and N_x and N_y are the number of nodes in the $x-$ and $y-$ axes, respectively.

4. One-dimensional IRBF discretisation of laminated composite plates

Let the subscripts bp and ip represent the location indices of boundary and interior points, N_{bp} the number of boundary points and N_{ip} the number of interior points.

Making use of (49), (50), (58), (59) and (60) and collocating the governing equations (17), (18) and (19) at the interior points result in

$$\left[\tilde{\mathbf{R}} - \lambda\,\tilde{\mathbf{S}}\right]\tilde{\phi} = \mathbf{0}, \tag{65}$$

where

$$\lambda = \omega^2, \tag{66}$$

$$\tilde{\mathbf{R}} = \begin{bmatrix} \begin{pmatrix} kA_{55}\tilde{\mathbf{D}}^{W}_{2x(ip,:)} \\ +kA_{44}\tilde{\mathbf{D}}^{W}_{2y(ip,:)} \end{pmatrix} & kA_{55}\tilde{\mathbf{D}}^{\Psi_x}_{1x(ip,:)} & kA_{44}\tilde{\mathbf{D}}^{\Psi_y}_{1y(ip,:)} \\ -kA_{55}\tilde{\mathbf{D}}^{W}_{1x(ip,:)} & \begin{pmatrix} D_{11}\tilde{\mathbf{D}}^{\Psi_x}_{2x(ip,:)} \\ +D_{66}\tilde{\mathbf{D}}^{\Psi_x}_{2y(ip,:)} - kA_{55}\mathbf{I} \end{pmatrix} & (D_{12}+D_{66})\tilde{\mathbf{D}}^{\Psi_y}_{2xy(ip,:)} \\ kA_{44}\tilde{\mathbf{D}}^{W}_{1y(ip,:)} & D_{66}\tilde{\mathbf{D}}^{\Psi_x}_{2xy(ip,:)} + D_{12}\tilde{\mathbf{D}}^{\Psi_x}_{2y(ip,:)} & \begin{pmatrix} D_{66}\tilde{\mathbf{D}}^{\Psi_y}_{2x(ip,:)} \\ +D_{22}\tilde{\mathbf{D}}^{\Psi_y}_{2y(ip,:)} - kA_{44}\mathbf{I} \end{pmatrix} \end{bmatrix}, \tag{67}$$

$$\tilde{\mathbf{S}} = \begin{bmatrix} I_0\mathbf{I} & \mathbf{0} & \mathbf{0} \\ \mathbf{0} & I_2\mathbf{I} & \mathbf{0} \\ \mathbf{0} & \mathbf{0} & I_2\mathbf{I} \end{bmatrix}, \tag{68}$$

$$\tilde{\phi} = \begin{bmatrix} \tilde{W} \\ \tilde{\psi}_x \\ \tilde{\psi}_y \end{bmatrix}, \tag{69}$$

and $\mathbf{I}$ and $\mathbf{0}$ are identity and zero matrices of dimensions $N_{ip}\times N$, respectively.

The system (65) can be expressed as

$$\tilde{\mathbf{L}}_G\tilde{\phi} = \lambda\tilde{\phi}, \tag{70}$$

where

$$\tilde{\mathbf{L}}_G = \tilde{\mathbf{S}}^{-1}\tilde{\mathbf{R}}. \tag{71}$$

Making use of (50) and (59) and collocating the expressions (22), (23) and (25) at the boundary points on Γ yield

$$\tilde{\mathbf{L}}_B\tilde{\phi} = \mathbf{0}, \tag{72}$$

where

$$\tilde{\mathbf{L}}_B = \begin{bmatrix} \mathbf{I} & \mathbf{0} & \mathbf{0} \\ \mathbf{0} & -n_y\mathbf{I} & n_x\mathbf{I} \\ \mathbf{0} & \begin{pmatrix} \left(n_x^2 D_{11} + n_y^2 D_{12}\right)\tilde{\mathbf{D}}_{1x(ip,:)} \\ +2n_x n_y D_{66}\tilde{\mathbf{D}}_{1y(ip,:)} \end{pmatrix} & \begin{pmatrix} \left(n_x^2 D_{12} + n_y^2 D_{22}\right)\tilde{\mathbf{D}}_{1y(ip,:)} \\ +2n_x n_y D_{66}\tilde{\mathbf{D}}_{1x(ip,:)} \end{pmatrix} \end{bmatrix}. \tag{73}$$

By combining (70) and (72), one is able to obtain the discrete form of 1D-IRBFN for laminated composite plates

$$\tilde{\mathbf{L}}_G\tilde{\phi} = \lambda\tilde{\phi}, \tag{74}$$

$$\tilde{\mathbf{L}}_B\tilde{\phi} = \mathbf{0}, \tag{75}$$

or

$$\begin{bmatrix} \tilde{\mathbf{L}}_{G(:,ip)} & \tilde{\mathbf{L}}_{G(:,bp)} \end{bmatrix} \begin{pmatrix} \tilde{\phi}_{(ip)} \\ \tilde{\phi}_{(bp)} \end{pmatrix} = \lambda\tilde{\phi}_{(ip)}, \tag{76}$$

$$\begin{bmatrix} \tilde{\mathbf{L}}_{B(:,ip)} & \tilde{\mathbf{L}}_{B(:,bp)} \end{bmatrix} \begin{pmatrix} \tilde{\phi}_{(ip)} \\ \tilde{\phi}_{(bp)} \end{pmatrix} = \mathbf{0}. \tag{77}$$

Solving (77) gives

$$\tilde{\phi}_{(bp)} = -\tilde{\mathbf{L}}_{B(:,bp)}^{-1}\tilde{\mathbf{L}}_{B(:,ip)}\tilde{\phi}_{(ip)}. \tag{78}$$

Substitution of (78) into (76) leads to the following system

$$\tilde{\mathbf{L}}\tilde{\phi}_{(ip)} = \lambda\tilde{\phi}_{(ip)}, \tag{79}$$

where $\tilde{\mathbf{L}}$ is a matrix of dimensions $N_{ip} \times N_{ip}$, defined as

$$\tilde{\mathbf{L}} = \tilde{\mathbf{L}}_{G(:,ip)} - \tilde{\mathbf{L}}_{G(:,bp)}\tilde{\mathbf{L}}_{B(:,bp)}^{-1}\tilde{\mathbf{L}}_{B(:,ip)}, \tag{80}$$

from which the natural frequencies and mode shapes of laminated composite plates can be obtained.

5. Numerical results and discussion

Three examples are considered here to study the performance of the present method. Unless otherwise stated, all layers of the laminate are assumed to be of the same thickness, density and made of the same linearly

elastic composite material. The material parameters of a layer used here are: $E_1/E_2 = 40$; $G_{12} = G_{13} = 0.6E_2$; $G_{23} = 0.5E_2$; $\nu_{12} = 0.25$, where the subscripts 1 and 2 denote the directions parallel and perpendicular to the fibre direction in a layer. The ply angle of each layer measured from the global $x-$ axis to the fibre direction is positive if measured clockwise, and negative if measured anti-clockwise. The eigenproblem (79) is solved using MATLAB to obtain the natural frequencies and mode shapes of laminated composite plates. In order to compare with the published results of Ferreira and Fasshauer [26], Liew [27], Liew et al. [33] and Nguyen-Van et al. [40], the same shear correction factors and nondimensionalised natural frequencies are also employed here:

- Case 1: Shear correction factor $K_s = \pi^2/12$
  Nondimensionalised natural frequency: $\bar{\omega} = \omega\,(b^2/\pi^2)\,\sqrt{\rho h/D_0}$ with $D_0 = E_2 h^3/12(1-\nu_{12}\nu_{21})$

- Case 2: Shear correction factor $K_s = 5/6$
  Nondimensionalised natural frequency: $\bar{\omega} = (\omega b^2/h)\,\sqrt{\rho/E_2}$

where b is the length of the vertical edges of square/rectangular plates or the diameter of circular plates. Boundary conditions can be imposed in the following ways:

- Approach 1: through the conversion process (39).

- Approach 2: by the algorithm (72) - (80).

5.1. Example 1: Rectangular laminated plates

This example investigates the characteristics of free vibration of rectangular cross-ply laminated plates with various thickness-to-length ratios, boundary conditions, lay-up stacking sequences and material properties. Both Approach 1 and Approach 2 are applied here to implement the boundary conditions.

5.1.1. Convergence study

Table 1 shows the convergence study of nondimensionalised natural frequencies. It can be seen that results by Approach 1 are slightly more accurate than those of Approach 2. The condition numbers in Approach 1 are smaller than those in Approach 2.

Table 2 presents the convergence study of nondimensionalised natural frequencies for simply supported three ply $[0^o/90^o/0^o]$ square and rectangular laminated plates for two cases of thickness to span ratios $t/b = 0.001$ and 0.2, while the corresponding convergence study for clamped laminated plates is presented in Table 3. Table 2 shows that faster convergence can be obtained for higher t/b ratios irrespective of a/b ratios. It can be seen that accuracy of the current results is generally higher than that of Ferreira and Fasshauer [26] who used RBF-pseudospectral method and nearly equal to that of Liew [27] in the case of $t/b = 0.2$. For the thin plate case $t/b = 0.001$, the p-Ritz method results are more accurate than RBF-pseudospectral ones and the IRBF ones in comparison with the exact solution. Specifically, the IRBF results of nondimensionalised fundamental natural frequency deviate by 0.32% from the exact solution for the simply supported plate, and by 0.05% from the p-Ritz method results for the clamped plate in the cases of $t/b = 0.001$ and $a/b = 1$.

5.1.2. Thickness-to-length ratios

Table 4 shows the effect of thickness-to-length ratio t/b on nondimensionalised fundamental frequency of the simply supported four-ply $[0^o/90^o/90^o/0^o]$ square laminated plate in comparison with other published results. It can be seen that the fundamental frequency decreases with increasing t/b ratios. The numerical results obtained are in good agreement with the published results of Liew [27] and Ferreira and Fasshauer [26] and the exact solution derived from the FSDT plate model [1]. Fig. 2 describes errors of nondimensionalised fundamental frequency $\varepsilon = (\bar{\omega} - \bar{\omega}_E)/\bar{\omega}_E$ ($\bar{\omega}_E$: nondimensionalised value of the exact fundamental frequency) with respect to thickness-to-span ratios t/b for the simply supported four-ply $[0^o/90^o/90^o/0^o]$ square laminated plate in comparison with available published results. This figure shows that the accuracy of the present method is higher than that of the others for t/b ratios larger than 0.04. The errors reduce with increasing t/b ratios for IRBFN and RBF-pseudospectral methods, indicating that these methods are more accurate for thick plates than for thin plates. When the t/b ratio is smaller than 0.04, the accuracy of p-Ritz method is higher than that of IRBF and RBF-pseudospectral methods.

5.1.3. Boundary conditions

Tables 5 and 6 show the effect of t/b ratio on nondimensionalised natural frequencies of three-ply $[0^o/90^o/0^o]$ and four-ply $[0^o/90^o/90^o/0^o]$ rectangular

laminated plates with boundary conditions SSSS, CCCC and SCSC. The first eight nondimensionalised natural frequencies are reported in these tables. It can be seen that the nondimensionalised natural frequencies reduce with increasing t/b ratios due to the effects of shear deformation and rotary inertia. These effects are more pronounced in higher modes. The effect of boundary conditions on the natural frequencies can also be seen in these tables. The higher constraints at the edges results in higher natural frequencies for the laminated plates as shown in Tables 5 and 6, i.e., the nondimensionalised natural frequency of SCSC plates is higher than that of SSSS plates, but lower than that of CCCC plates. Fig. 3-5 show mode shapes of a simply supported three-ply $[0^o/90^o/0^o]$ square laminated plate, a simply supported three-ply $[0^o/90^o/0^o]$ rectangular with $a/b = 2$ laminated plate, and a clamped three-ply $[0^o/90^o/0^o]$ square laminated plate, respectively, in the case of $t/b = 0.2$ and using a grid of 15×15. The current results are fairly reasonable in comparison with available published results [26].

5.1.4. Material property

Tables 7 presents the effect of modulus ratio E_1/E_2 on the nondimensionalised fundamental frequency of the simply supported four-ply $[0^o/90^o/90^o/0^o]$ square laminated plate. In order to compare with the available published results, the shear correction factor of 5/6 and thickness-to-length ratio of 0.2 are used in this example. It can be seen that the fundamental frequency increases with increasing modulus ratio. Fig. 6 shows the errors of nondimensionalised fundamental frequency ($\varepsilon = (\bar{\omega} - \bar{\omega}_E)/\bar{\omega}_E$) with respect to modulus ratio E_1/E_2 for the simply supported four-ply laminated square plate $[0^o/90^o/90^o/0^o]$ in comparison with existing published results. The accuracy of current method is not only fairly high but also very stable in a wide range of E_1/E_2 ratio as shown in this figure.

5.2. Example 2: Circular laminated plates

Free vibration analysis for $[\beta^o/-\beta^o/-\beta^o/\beta^o]$ circular laminated plates with diameter b and thickness t shown in Fig. 7 is studied in this section. Boundary conditions are imposed with Approach 2. The thickness-to-diameter ratio t/b of 0.1, various fibre orientation angles with $\beta = 0^o$ and 45^o, and modulus ratio (E_1/E_2) of 40 are considered. Tables 8 presents the convergence study of nondimensionalised natural frequencies for various mode numbers for the simply supported four-ply $[\beta^o/-\beta^o/-\beta^o/\beta^o]$ circular laminated plate in comparison with other published results, while the

corresponding convergence study for a clamped four-ply $[\beta^o/-\beta^o/-\beta^o/\beta^o]$ circular laminated plate is given in Tables 9. It can be seen that the current results are in good agreement with those of Liew et al. [33] who used a moving least squares differential quadrature method (MLSDQ). The numerical solution converges faster for the clamped circular plate than for the simply supported one. Tables 10 shows the effect of thickness-to-diameter ratio on the nondimensionalised frequencies for various modes of the clamped four ply $[\beta^o/-\beta^o/-\beta^o/\beta^o]$ circular laminated plate. A grid is taken to be 15×15 in this computation. Fig. 8 presents the mode shapes of the simply supported four-ply $[45^o/-45^o/-45^o/45^o]$ circular laminated plate with $t/b=0.1$.

5.3. Example 3: Square isotropic plate with a square hole

Before investigating the free vibration of a square isotropic plate with a square hole for which there is currently no exact solution, a simply supported square isotropic plate is considered to validate the results of both 1D-IRBF method and Strand7 (Finite element analysis system) [41]. The results by the 1D-IRBF for complete geometries can then be compared with those obtained by Strand7. Approach 1 is employed here to implement the boundary conditions. Tables 11 presents the comparison of nondimensionalised natural frequencies between 1D-IRBF, Strand7 and exact results for the simply supported square isotropic plate with thickness to length ratio t/b of 0.1. Converged solutions are obtained on a grid of 15×15 for the IRBF method and of 21×21 for Strand7. This table shows that the IRBF result is more accurate than Strand7's in comparison with the exact solution of Reddy [1]. Next, the methods are used to analyse the simply supported square isotropic plate with a square hole. All edges of the hole are also subjected to the simply supported boundary condition. Tables 12 shows the nondimensionalised natural frequencies for various mode numbers of the simply supported square isotropic plate with a square hole. In this computation, the grid is taken to be 17×17 for the IRBF method and 41×41 for Strand7 to obtain the converged solutions. It can be seen that good agreement between the 1D-IRBF and Strand7 results is obtained for various mode numbers. Fig. 9 shows the first four mode shapes of the simply supported square isotropic plate with a square hole.

6. Conclusions

Free vibration analysis of laminated composite plates using FSDT and 1D-IRBFN method is presented. Unlike DRBFNs, IRBFNs are constructed through integration rather than differentiation, which helps to stabilise a numerical solution and provide an effective way to implement derivative boundary conditions. Cartesian grids are used to discretise both rectangular and non-rectangular plates. The laminated composite plates with various boundary conditions, length-to-width ratios a/b, thickness-to-length ratios t/b, and material properties are considered. The obtained numerical results are in good agreement with the available published results and exact solutions. Convergence study shows that faster rates are obtained for higher t/b ratios irrespective of a/b ratios of the rectangular plates. The effects of boundary conditions on the natural frequencies are also numerically investigated, which indicates that higher constraints at the edges yield higher natural frequencies. It is also found that the present method is not only highly accurate but also very stable for a wide range of modulus ratio.

7. Acknowledgements

This research is supported by the University of Southern Queensland, Australia through a USQ Postgraduate Research Scholarship awarded to D. Ngo-Cong. We would like to thank the reviewers for their helpful comments.

References

[1] Reddy JN. Mechanics of Laminated Composite Plates and Shells: Theory and Analysis (second edition). London: CRC Press; 2004.

[2] Noor AK, Burton WS. Free Vibration of Multilayered Composite Plates. AIAA J 1973; 11: 1038-39.

[3] Srinivas S, Rao AK. Bending, vibration and buckling of simply supported thick orthotropic rectangular plates and laminates. Int J Solids Struct 1970; 6(11): 1463-81.

[4] Liew KM, Hung KC, Lim MK. A Continuum Three-dimensional Vibration Analysis of Thick Rectangular Plates. Int J Solids Struct 1993; 30(24): 3357-79.

[5] Liew KM, Hung KC, Lim MK. Three-Dimensional Vibration of Rectangular Plates: Variance of Simple support conditions and influence of In-lane Inertia. Int J Solids Struct 1994; 31(23): 3233-3247.

[6] Liew KM, Hung KC, Lim MK. Three-Dimensional Vibration of Rectangular Plates: Effects of Thickness and Edge Constraints. J Sound Vib 1995; 182(5): 709-27.

[7] Liew KM, Teo TM. Three-Dimensional Vibration Analysis of Rectangular Plates based on Differential Quadrature Method. J Sound Vib 1999; 220(4): 577-599.

[8] Reddy JN, Phan ND. Stability and Vibration of Isotropic, Orthotropic and Laminated Plates according to a Higher-Order Shear Deformation Theory. J Sound Vib 1985; 98: 157-70.

[9] Reddy JN. A simple higher-order theory for laminated composite plates. J Appl Mech 1984; 51: 745-752.

[10] Lim CW, Liew KM, Kitipornchai S. Numerical Aspects for Free Vibration of Thick Plates. Part I: Formulation and Verification. Comput Methods Appl Mech Eng 1998; 156: 15-29.

[11] Lim CW, Liew KM, Kitipornchai S. Numerical Aspects for Free Vibration of Thick Plates. Part II: Numerical Efficiency and Vibration Frequencies. Comput Methods Appl Mech Eng 1998; 156: 31-44.

[12] Liu GR. Meshfree Methods: Moving Beyond the Finite Element Method. London: CRC Press; 2003.

[13] Nayroles B, Touzot G, Villon P. Generalizing the Finite Element Method: Diffuse Approximation and Diffuse Elements. Comput Mech 1992; 10: 307-18.

[14] Belytschko T, Lu YY, Gu L. Element-Free Galerkin Methods. Int J Numer Methods Eng 1994; 37: 229-56.

[15] Atluri SN, Zhu T. A new Meshless Local Petrov-Galerkin (MLPG) Approach in Computational Mechanics. Comput Mech 1998; 22: 117-27.

[16] Liu GR, Gu YT. A Point Interpolation Method for Two-Dimensional Solids. Int J Numer Methods Eng 2001; 50: 937-51.

[17] Wang JG, Liu GR. A Point Interpolation Meshless Method based on Radial Basis Function. Int J Numer Methods Eng 2002; 54: 1623-48.

[18] Liew KM, Chen XL. Buckling of rectangular Mindlin Plates subjected to Partial In-plane Edge loads using the Radial Point Interpolation Method. Int J Solids Struct 2004; 41: 1677-95.

[19] Liew KM, Chen XL, Reddy JN. Mesh-free Radial Basis Function Method for Buckling Analysis of Non-uniformly Loaded Arbitrarily Shaped Shear Deformable Plates. Comput Methods Appl Mech Eng 2004; 193: 205-24.

[20] Liu GR, Zhang GY, Dai KY. A Linearly Conforming Point Interpolation Method (LC-PIM) for 2D Solid Mechanics Problems. Int J Comput Methods 2005; 2(4): 645-65.

[21] Liu GR, Li Y, Dai KY. A linearly Conforming Radial Point Interpolation Method for Solid Mechanics Problems. Int J Comput Methods 2006; 3(4): 401-28.

[22] Kansa EJ. Multiquadrics - A Scattered Data Approximation Scheme with Applications to Computational Fulid-Dynamics - I: Surface Approximations and Partial Derivative Estimates. Comput Math Appl 1990; 19(8/9): 127-45.

[23] Kansa EJ. Multiquadrics - A Scattered Data Approximation Scheme with Applications to Computational Fulid-Dynamics - II: Solutions to parabolic, Hyperbolic and Elliptic Partial Differential Equations. Comput Math Appl 1990; 19(8/9): 147-61.

[24] Ferreira AJM, Roque CMC, Jorge RMN. Free Vibration Analysis of Symmetric Laminated Composite Plates by FSDT and Radial Basis Functions. Comput Methods Appl Mech Eng 2005; 194: 4265-78.

[25] Ferreira AJM, Fasshauer GE. Free Vibration Analysis of Timoshenko Beams and Mindlin Plates by Radial Basis Functions. Int J Compt Methods 2005; 2(1): 15-31.

[26] Ferreira AJM, Fasshauer GE. Analysis of Natural Frequencies of Composite Plates by an RBF-Pseudospectral Method. Compos Struct 2007; 79: 202-10.

[27] Liew KM. Solving the Vibration of Thick Symmetric Laminates by Reissner/Mindlin Plates Theory and the p-Ritz Method. J Sound Vib 1996; 198(3): 343-60.

[28] Karunasena W, Liew KM, Al-Bermani FGA. Natural Frequencies of Thick Arbitrary Quadrilateral Plates using the pb-2 Ritz Method. J Sound Vib 1996; 196(4): 371-85.

[29] Karunasena W, Kitipornchai S. Free Vibration of Shear-Deformable General Triangular Plates. J Sound Vib 1997; 199(4): 595-613.

[30] Liew KM, Ng TY, Zhao X, Reddy JN. Harmonic reproducing kernel particle method for free vibration of rotating cylindrical shells. Comput Methods Appl Mech Eng 2002; 191: 4141-57.

[31] Zhao X, Ng TY, Liew KM. Free Vibration of Two-Side Simply-Supported Laminated Cylindrical Panels via the Mesh-free kp-Ritz Method. Int J Mech Sci 2004; 46: 123-42.

[32] Liew KM, Wang J, Tan MJ, Rajendran S. Nonlinear Analysis of Laminated Composite Plates using the Mesh-free kp-Ritz Method based on FSDT. Comput Methods Appl Mech Eng 2004; 193: 4763-79.

[33] Liew KM, Huang YQ, Reddy JN. Vibration Analysis of Symmetrically Laminated Plates based on FSDT using the Moving Least Squares Differential Quadrature Method. Comput Methods Appl Mech Eng 2003; 192: 2203-22.

[34] Liew KM, Wang J, Ng TY, Tan MJ. Free Vibration and Buckling Analyses Of Shear-Deformable Plates based on FSDT Meshfree Method. J Sound Vib 2004; 276: 997-1017.

[35] Mai-Duy N, Tran-Cong T. Numerical Solution of Navier-Stokes Equations using Multiquadric Radial Basis Function Networks. Int J Numer Methods Fluids 2001; 37: 65-86.

[36] Mai-Duy N, Tran-Cong T. Approximation of Function and Its Derivatives using Radial Basis Function Networks. Appl Math Model 2003; 27: 197-220.

[37] Mai-Duy N, Tran-Cong T. Indirect RBFN Mehtod with Thin Plate Splines for Numerical Solution of Differential Equations. Comput Model Eng Sci 2003; 4(1): 85-102.

[38] Mai-Duy N, Khennane A, Tran-Cong T. Computation of Laminated Composite Plates using Integrated Radial Basis Function Networks. Comput Mater Continua 2007; 5(1): 63-77.

[39] Mai-Duy N, Tanner RI. A Collocation Method based on One-Dimensional RBF Interpolation Scheme for Solving PDEs. Int J Numer Methods Heat Fluid Flow 2007; 17(2): 165-86.

[40] Nguyen-Van H, Mai-Duy N, Tran-Cong T. Free Vibration Analysis of Laminated Plate/Shell Structures Based on FSDT with a Stabilized Nodal-Integrated Quadrilateral Element. J Sound Vib 2008; 313: 205-23.

[41] Strand7 online help. Finite element analysis system. Release 2.3.7; 2005.

Table 1: Simply supported three-ply $[0^o/90^o/0^o]$ square laminated plate: convergence study of nondimensionalised natural frequencies $\bar{\omega} = \omega \left(b^2/\pi^2\right) \sqrt{\rho h/D_0}$ by two approaches, $t/b = 0.2$.

		Mode sequence number								
	Grid	1	2	3	4	5	6	7	8	Condition number
Approach 1	11x11	3.5939	5.7708	7.3982	8.6896	9.1665	11.2222	11.2406	12.1306	1.36E+05
	13x13	3.5939	5.7696	7.3974	8.6881	9.1520	11.2125	11.2283	12.1209	2.43E+05
	15x15	3.5939	5.7693	7.3972	8.6878	9.1478	11.2097	11.2248	12.1182	3.95E+05
	17x17	3.5939	5.7692	7.3971	8.6876	9.1463	11.2087	11.2235	12.1173	5.65E+05
Approach 2	11x11	3.5932	5.7649	7.3968	8.6851	9.1299	11.2111	11.2184	12.1252	2.60E+05
	13x13	3.5935	5.7667	7.3967	8.6860	9.1371	11.2108	11.2162	12.1186	9.21E+05
	15x15	3.5937	5.7676	7.3968	8.6865	9.1402	11.2088	11.2186	12.1169	2.45E+06
	17x17	3.5937	5.7681	7.3969	8.6868	9.1418	11.2082	11.2199	12.1165	5.12E+06
Exact [1]		3.5939	5.7691	7.3972	8.6876	9.1451	11.2080	11.2230	12.1170	

Table 2: Simply supported three-ply $[0^o/90^o/0^o]$ rectangular laminated plate: convergence study of nondimensionalised natural frequencies $\bar{\omega} = \omega\left(b^2/\pi^2\right)\sqrt{\rho h/D_0}$. Note that Ferreira and Fasshauer [26] used 19x19 grid.

			Mode sequence number							
a/b	t/b	Grid	1	2	3	4	5	6	7	8
1	0.001	11x11	6.6542	9.4811	15.9414	24.983	26.3037	26.3794	30.0499	37.4233
		13x13	6.6427	9.4708	16.0981	25.0024	26.2019	26.3967	30.1587	37.3711
		15x15	6.6592	9.4715	16.1697	24.9665	26.3591	26.4214	30.1662	37.5117
		17x17	6.6464	9.466	16.2146	24.8845	26.2837	26.534	30.1281	37.5459
		Ferreira and Fasshauer [26]	6.618	9.4368	16.2192	25.1131	26.4938	26.6667	30.2983	37.785
		Liew (p-Ritz) [27]	6.6252	9.447	16.2051	25.1146	26.82	26.6572	30.3139	37.7854
		Exact [1]	6.6252	9.447	16.205	25.115	26.498	26.657	30.314	37.785
	0.2	11x11	3.5939	5.7708	7.3982	8.6896	9.1665	11.2222	11.2406	12.1306
		13x13	3.5939	5.7696	7.3974	8.6881	9.152	11.2125	11.2283	12.1209
		15x15	3.5939	5.7693	7.3972	8.6878	9.1478	11.2097	11.2248	12.1182
		17x17	3.5939	5.7692	7.3971	8.6876	9.1463	11.2087	11.2235	12.1173
		Ferreira and Fasshauer [26]	3.5934	5.7683	7.3968	8.867	9.1444	11.2078	11.2218	12.1162
		Liew (p-Ritz) [27]	3.5939	5.7691	7.3972	8.6876	9.1451	11.208	11.2225	12.1166
		Exact [1]	3.5939	5.7691	7.3972	8.6876	9.1451	11.208	11.223	12.117
2	0.001	11x11	2.3728	6.6869	6.7991	8.3924	9.6042	13.9864	14.0793	15.8732
		13x13	2.3866	6.7419	6.7685	9.599	14.393	14.533	16.2707	16.3855
		15x15	2.3855	6.7206	6.7569	9.575	14.4173	14.5091	16.2875	16.354
		17x17	2.3641	6.6461	6.671	9.4658	14.2607	14.386	16.1137	16.2146
		Ferreira and Fasshauer [26]	2.367	6.6331	6.6691	9.4676	14.2921	14.3915	16.1009	16.1009
		Liew (p-Ritz) [27]	2.3618	6.6252	6.6845	9.447	14.2869	16.3846	16.1347	16.2051
		Exact [1]	2.3618	6.6252	6.6645	9.447	14.287	14.3846	16.1347	16.2051
	0.2	11x11	1.9393	3.5945	4.8775	5.4933	5.7712	7.125	7.457	8.6202
		13x13	1.9393	3.594	4.8761	5.488	5.7697	7.12	7.4118	8.6047
		15x15	1.9393	3.5939	4.8757	5.4864	5.7693	7.1186	7.4022	8.6003
		17x17	1.9393	3.5939	4.8756	5.4859	5.7692	7.1181	7.3992	8.5987
		Ferreira and Fasshauer [26]	1.9387	3.5934	4.875	5.4851	5.7683	7.117	7.3968	8.5969
		Liew (p-Ritz) [27]	1.9393	3.5939	4.8755	5.4855	5.7691	7.1177	7.3972	8.5973
		Exact [1]	1.9393	3.5939	4.8755	5.4855	5.7691	7.1177	7.3972	8.5973

Table 3: Clamped three-ply $[0^o/90^o/0^o]$ rectangular laminated plate: convergence study of nondimensionalised natural frequencies $\bar{\omega} = \omega \left(b^2/\pi^2\right) \sqrt{\rho h/D_0}$. Note that Ferreira and Fasshauer [26] used 19x19 grid.

			Mode sequence number							
a/b	t/b	Grid	1	2	3	4	5	6	7	8
1	0.001	11x11	14.6844	17.6511	24.1628	33.6225	39.0914	40.7855	44.6870	51.2194
		13x13	14.6791	17.6539	24.3897	34.7431	39.1978	40.8591	44.8533	47.8648
		15x15	14.6774	17.6470	24.4898	35.2604	39.2082	40.8519	44.8829	48.8046
		17x17	14.6722	17.6383	24.5238	35.4471	39.2005	40.8349	44.8746	49.5902
		Ferreira and Fasshauer [26]	14.8138	17.6138	24.5114	35.5318	39.1572	40.7685	44.7865	50.3226
		Liew (p-Ritz) [27]	14.6655	17.6138	24.5114	35.5318	39.1572	40.7685	44.7865	50.3226
	0.2	11x11	4.4466	6.6433	7.7006	9.1870	9.7502	11.4125	11.6550	12.4789
		13x13	4.4466	6.6423	7.6998	9.1856	9.7417	11.4033	11.6473	12.4698
		15x15	4.4466	6.6420	7.6996	9.1853	9.7393	11.4007	11.6452	12.4673
		17x17	4.4466	6.6419	7.6996	9.1852	9.7384	11.3998	11.6444	12.4664
		Ferreira and Fasshauer [26]	4.4463	6.6419	7.6995	9.1839	9.7376	11.3994	11.6420	12.4651
		Liew (p-Ritz) [27]	4.4468	6.6419	7.6996	9.1852	9.7378	11.3991	11.6439	12.4658
2	0.001	11x11	5.1181	10.5213	10.5731	14.3641	19.1429	19.1845	21.8532	21.8669
		13x13	5.1140	10.5488	10.6073	14.3851	19.4334	19.4949	22.0916	22.1203
		15x15	5.1140	10.5491	10.6086	14.3748	19.5293	19.6364	22.1586	22.2252
		17x17	5.1092	10.5447	10.6042	14.3642	19.5622	19.6912	22.1764	22.2607
		Liew (p-Ritz) [27]	5.1051	10.5265	10.5828	14.3241	19.5674	19.7011	22.1483	22.2368
	0.2	11x11	3.0454	4.2489	5.7933	5.9109	6.5371	7.7354	7.7434	9.1903
		13x13	3.0454	4.2485	5.7921	5.9066	6.5358	7.7016	7.7311	9.1813
		15x15	3.0454	4.2484	5.7918	5.9054	6.5354	7.6927	7.7300	9.1787
		17x17	3.0453	4.2484	5.7917	5.9050	6.5353	7.6900	7.7295	9.1778
		Liew (p-Ritz) [27]	3.0453	4.2484	5.7918	5.9047	6.5354	7.6881	7.7293	9.1762

Table 4: Simply supported four-ply $[0^o/90^o/90^o/0^o]$ square laminated plate: effect of thickness-to-length ratio on the nondimensionalised fundamental frequency $\bar{\omega} = \omega \left(b^2/\pi^2\right) \sqrt{\rho h/D_0}$ in comparison with other published results, using a grid of 13×13.

t/b	0.01	0.0200	0.04	0.05	0.08	0.1	0.2	0.25
IRBFN	6.6069	6.5464	6.3378	6.1882	5.6675	5.2991	3.7918	3.2806
Liew (p-Ritz) [27]	6.6060	6.5490	6.3380	6.1930	5.6770	5.3110	3.8070	3.2950
Ferreira and Fasshauer [26]	6.6012	6.5438	6.3300	6.1844	5.6641	5.2960	3.7903	3.2796
Exact [1]	6.6059	6.5483	6.3342	6.1885	5.6675	5.2991	3.7918	3.2806

Table 5: Three-ply $[0^o/90^o/0^o]$ rectangular laminated plates with various boundary conditions: effect of thickness-to-length ratio on nondimensionalised natural frequencies $\bar{\omega} = \omega \left(b^2/\pi^2\right) \sqrt{\rho h/D_0}$, using a grid of 13×13.

			Mode sequence number							
B.C.	a/b	t/b	1	2	3	4	5	6	7	8
SSSS	1	0.001	6.6427	9.4708	16.0981	25.0024	26.2019	26.3967	30.1587	37.3711
		0.050	6.1379	10.4509	12.2686	12.2686	14.9902	19.3564	20.7612	24.2701
		0.100	5.1662	7.7586	12.9473	13.0492	14.3770	17.8115	19.6232	21.0611
		0.150	4.2748	6.6678	9.4883	10.8246	10.8377	13.8136	14.6715	15.5964
		0.200	3.5939	5.7696	7.3974	8.6881	9.1520	11.2125	11.2283	12.1209
	2	0.001	2.3866	6.7419	6.7685	9.5990	14.3930	14.5330	16.2707	16.3855
		0.050	2.3251	6.1374	6.5306	8.9272	11.4203	12.1885	13.4651	14.0131
		0.100	2.2213	5.1659	6.0163	7.7562	9.0282	10.8012	11.8844	12.9471
		0.150	2.0855	4.2751	5.4445	6.6679	6.8725	8.5997	9.5089	10.0955
		0.200	1.9393	3.5940	4.8761	5.4880	5.7697	7.1200	7.4118	8.6047
CCCC	1	0.001	14.6791	17.6539	24.3897	34.7431	39.1978	40.8591	44.8533	47.8648
		0.050	10.9532	14.0298	20.3988	23.1977	24.9817	29.2481	29.4098	36.3054
		0.100	7.4108	10.3935	13.9134	15.4372	15.8068	19.5792	21.4976	21.6743
		0.150	5.5482	8.1470	9.9044	11.6223	12.0305	14.6493	14.9165	16.1288
		0.200	4.4466	6.6423	7.6998	9.1856	9.7417	11.4033	11.6473	12.4698
	2	0.001	5.1140	10.5488	10.6073	14.3851	19.4334	19.4949	22.0916	22.1203
		0.050	4.7791	8.8414	9.8490	12.5142	14.7127	17.3115	17.6840	19.4410
		0.100	4.1412	6.6172	8.3548	9.8967	9.9710	12.4472	13.6882	14.1293
		0.150	3.5397	5.1819	6.9271	7.4270	7.9371	9.5807	9.8737	11.2359
		0.200	3.0454	4.2485	5.7921	5.9066	6.5358	7.7016	7.7311	9.1813
SCSC	1	0.001	7.4203	12.1879	20.6756	25.2643	27.6224	32.1561	33.0467	42.0340
		0.050	6.8909	11.2486	18.6756	19.6220	21.8062	26.7027	28.3039	34.3921
		0.100	5.8707	9.4551	13.3411	14.8865	15.3416	19.2365	21.2412	21.3301
		0.150	4.9054	7.7815	9.7801	11.5266	11.8206	14.5809	14.8557	16.0790
		0.200	4.1370	6.4758	7.6655	9.1608	9.6559	11.3907	11.6364	12.4619
	2	0.001	3.9926	7.4338	10.0811	12.1967	14.5705	17.8531	19.1850	20.6813
		0.050	3.8663	6.8929	9.4403	11.2497	12.5959	15.6065	17.4616	18.6763
		0.100	3.5695	5.8712	8.1101	9.4478	9.4554	12.0675	13.3765	14.0007
		0.150	3.2017	4.9056	6.7853	7.2757	7.7816	9.4780	9.8001	11.1627
		0.200	2.8400	4.1370	5.7076	5.8509	6.4748	7.6786	7.6951	9.1385

Table 6: Four-ply $[0^o/90^o/90^o/0^o]$ rectangular laminated plates with various boundary conditions: effect of thickness-to-length ratio on nondimensionalised natural frequency $\bar{\omega} = \omega \left(b^2/\pi^2\right) \sqrt{\rho h/D_0}$, using a grid of 13×13.

			Mode sequence number							
B.C.	a/b	t/b	1	2	3	4	5	6	7	8
SSSS	1	0.001	6.7059	12.0397	18.5141	22.0534	23.3726	30.9024	40.5234	46.2463
		0.050	6.1882	11.1007	18.8131	20.7977	21.2014	27.7936	33.4569	34.3564
		0.100	5.2991	9.5066	12.8655	15.1686	16.3195	20.1927	20.7286	22.2630
		0.150	4.4572	7.9529	9.4381	11.5313	12.8403	14.5062	15.3210	15.9592
		0.200	3.7918	6.6928	7.4020	9.2365	10.3860	11.1171	12.1797	12.4176
	2	0.001	2.9712	6.6541	9.9919	11.9088	13.6687	17.1813	21.8132	22.9920
		0.050	2.9126	6.1904	9.4342	11.1019	11.8981	15.2281	18.9543	19.8146
		0.100	2.7737	5.2996	8.2610	8.9588	9.5069	11.9952	12.9014	15.1988
		0.150	2.5834	4.4575	6.9071	7.0351	7.9531	9.4582	9.5600	11.5477
		0.200	2.3764	3.7920	5.5656	5.9910	6.6929	7.4160	7.8395	9.2477
CCCC	1	0.001	14.6792	20.6910	32.9201	37.6858	40.8607	48.8204	50.1301	62.4002
		0.050	11.3126	16.7726	22.9297	26.2097	26.2696	33.2400	37.0230	38.2915
		0.100	7.8902	12.1365	13.9783	16.8124	18.3066	21.3197	21.7360	23.3033
		0.150	5.9351	9.1657	9.9964	12.2341	13.5791	14.8417	15.8326	16.4452
		0.200	4.7214	7.2800	7.7663	9.5679	10.7005	11.3499	12.3791	12.6607
	2	0.001	6.5340	10.9786	15.6695	18.2386	19.0696	24.2980	29.7601	29.9145
		0.050	6.0569	9.3919	13.6991	14.7711	15.5837	19.4157	21.3104	24.3658
		0.100	5.1020	7.1586	10.2158	10.5241	11.7065	13.7411	13.8243	16.6254
		0.150	4.1965	5.5887	7.6416	8.1429	8.9674	9.9607	10.3876	12.2071
		0.200	3.4843	4.5283	6.0592	6.5421	7.1725	7.7662	8.2341	9.5683
SCSC	1	0.001	8.3209	16.7088	24.5146	29.0185	30.5059	39.2791	48.5199	53.3015
		0.050	7.7027	14.6439	19.3708	23.2436	25.0077	31.0304	34.6669	37.0746
		0.100	8.2781	16.5860	24.2823	28.7169	30.3815	38.9510	48.8953	52.1464
		0.150	8.2468	16.4639	24.0415	28.4167	30.0368	38.4583	48.1057	49.8091
		0.200	4.4165	7.1096	7.7278	9.5387	10.5949	11.3260	12.3570	12.6413
	2	0.001	5.7766	8.3309	14.5915	15.3473	16.7142	20.8753	24.1291	28.6815
		0.050	5.4215	7.7045	12.7571	13.4298	14.6448	17.9696	19.5078	23.3567
		0.100	4.6716	6.4819	9.6960	10.3349	11.3299	13.4182	13.4679	16.3745
		0.150	3.9187	5.3244	7.4861	8.0180	8.8189	9.8824	10.2831	12.1477
		0.200	3.3028	4.4166	6.0005	6.4606	7.1096	7.7412	8.1954	9.5496

Table 7: Simply supported four-ply $[0^o/90^o/90^o/0^o]$ square laminated plate: effect of modulus ratio E_1/E_2 on the accuracy of nondimensionalised fundamental frequency $\bar{\omega} = \left(\omega b^2/h\right)\sqrt{\rho/E_2}$, $t/b = 0.2$, using a grid of 13×13, $K_s = 5/6$.

	E_1/E_2			
	10	20	30	40
IRBFN	8.2982	9.5671	10.3258	10.8540
Nguyen-Van et al. (MISQ20) [40]	8.3094	9.5698	10.3224	10.8471
Liew et al. (MLSDQ) [33]	8.2992	9.5680	10.3270	10.8550
Exact [1]	8.2982	9.5671	10.3260	10.8540

Table 8: Simply supported four-ply $[\beta^o/-\beta^o/-\beta^o/\beta^o]$ circular laminated plate: convergence study of nondimensionalised natural frequencies for various mode number $\bar{\omega} = \left(\omega b^2/h\right)\sqrt{\rho/E_2}$, $t/b = 0.1$, $E_1/E_2 = 40$.

		Mode sequence number							
β	Grid	1	2	3	4	5	6	7	8
0^o	11x11	16.720	24.339	36.233	41.031	49.048	52.850	60.710	65.304
	13x13	16.690	24.157	35.490	40.980	48.803	50.483	59.661	65.091
	15x15	16.673	24.083	35.215	40.952	48.707	49.640	59.293	64.959
	17x17	16.664	24.046	35.084	40.936	48.659	49.254	59.124	64.833
	19x19	16.658	24.025	35.014	40.926	48.631	49.056	59.032	64.709
	25x25	16.648	23.999	34.931	40.910	48.592	48.838	58.919	64.473
	31x31	16.645	23.990	34.904	40.904	48.576	48.774	58.878	64.384
	Nguyen-Van et al. (MISQ20) [40]	16.168	-	-	-	-	-	-	-
	Liew et al. (MLSDQ, $N_c = 3$) [33]	16.512	-	-	-	-	-	-	-
	Liew et al. (MLSDQ, $N_c = 4$) [33]	16.359	-	-	-	-	-	-	-
	Liew et al. (MLSDQ, $N_c = 5$) [33]	16.278	-	-	-	-	-	-	-
45^o	11x11	17.653	32.175	40.886	52.412	53.679	64.551	71.124	72.677
	13x13	17.643	32.128	40.861	52.116	53.683	64.376	70.979	72.288
	15x15	17.637	32.111	40.847	51.997	53.682	64.304	70.898	72.055
	17x17	17.634	32.103	40.839	51.939	53.679	64.267	70.852	71.926
	19x19	17.631	32.098	40.833	51.907	53.677	64.246	70.824	71.853
	25x25	17.627	32.090	40.824	51.866	53.670	64.218	70.784	71.762
	31x31	17.625	32.087	40.819	51.850	53.665	64.208	70.767	71.732
	Nguyen-Van et al. (MISQ20) [40]	17.162	-	-	-	-	-	-	-
	Liew et al. (MLSDQ, $N_c = 3$) [33]	17.147	-	-	-	-	-	-	-
	Liew et al. (MLSDQ, $N_c = 4$) [33]	17.781	-	-	-	-	-	-	-
	Liew et al. (MLSDQ, $N_c = 5$) [33]	17.141	-	-	-	-	-	-	-

Table 9: Clamped four-ply $[\beta^o/-\beta^o/-\beta^o/\beta^o]$ circular laminated plate: convergence study of nondimensionalised natural frequencies for various mode number $\left(\bar{\omega} = \left(\omega b^2/h\right)\sqrt{\rho/E_2},\ t/b = 0.1,\ E_1/E_2 = 40\right)$.

		Mode sequence number							
β	Grid	1	2	3	4	5	6	7	8
0^o	11x11	22.198	29.658	40.987	42.764	50.582	55.075	61.568	65.849
	13x13	22.195	29.647	40.929	42.754	50.521	54.906	61.299	65.793
	15x15	22.198	29.646	40.921	42.759	50.526	54.876	61.312	65.787
	17x17	22.198	29.644	40.918	42.761	50.523	54.865	61.304	65.786
	Nguyen-Van et al. (MISQ20) [40]	22.123	29.768	41.726	42.805	50.756	56.950	-	-
	Liew et al. (MLSDQ, $N_c = 3$) [33]	22.211	29.651	41.101	42.635	50.309	54.553	60.719	64.989
	Liew et al. (MLSDQ, $N_c = 4$) [33]	22.219	-	-	-	-	-	-	-
	Liew et al. (MLSDQ, $N_c = 5$) [33]	22.199	-	-	-	-	-	-	-
45^o	11x11	24.737	39.112	43.638	57.190	57.254	65.693	74.254	75.149
	13x13	24.737	39.101	43.630	57.135	57.194	65.640	74.029	74.854
	15x15	24.737	39.099	43.630	57.138	57.185	65.630	74.035	74.823
	17x17	24.737	39.099	43.630	57.136	57.181	65.627	74.029	74.810
	Nguyen-Van et al. (MISQ20) [40]	24.766	39.441	43.817	57.907	57.945	66.297	-	-
	Liew et al. (MLSDQ, $N_c = 3$) [33]	24.752	39.181	43.607	56.759	56.967	65.571	73.525	74.208
	Liew et al. (MLSDQ, $N_c = 4$) [33]	24.744	-	-	-	-	-	-	-
	Liew et al. (MLSDQ, $N_c = 5$) [33]	24.734	-	-	-	-	-	-	-

Table 10: Clamped four-ply $[\beta^o/-\beta^o/-\beta^o/\beta^o]$ circular laminated plate: effect of thickness-to-diameter ratio on nondimensionalised natural frequencies for various mode numbers, $\bar{\omega} = \left(\omega b^2/h\right)\sqrt{\rho/E_2}$, $E_1/E_2 = 40$, using a grid of 15×15.

		Mode sequence number							
β	t/b	1	2	3	4	5	6	7	8
0^o	0.001	45.245	56.510	72.646	93.440	118.647	119.399	134.972	146.804
	0.050	33.401	42.190	55.649	70.957	73.602	80.909	94.742	95.602
	0.100	22.198	29.646	40.921	42.759	50.526	54.876	61.312	65.787
	0.150	16.424	23.040	30.528	32.359	37.045	43.081	45.728	45.907
	0.200	13.111	18.923	23.801	26.641	29.339	35.109	35.246	36.465
45^o	0.001	46.435	70.615	110.019	115.873	143.115	163.166	184.000	218.970
	0.050	35.506	55.366	70.743	84.208	89.932	112.326	117.096	117.614
	0.100	24.737	39.099	43.630	57.138	57.185	65.630	74.035	74.823
	0.150	18.580	29.222	31.328	41.286	41.855	46.084	53.062	53.211
	0.200	14.754	23.093	24.359	32.151	32.686	35.454	41.023	41.079

Table 11: Simply supported square isotropic plate: Comparison of nondimensionalised natural frequencies among 1D-IRBF, Strand7 and exact results, $\bar{\omega} = \left(\omega b^2/h\right)\sqrt{\rho/E_2}$, $t/b = 0.1$, $K_s = 5/6$.

Mode	IRBF (15×15)	Strand7 (21×21)	Exact [1]
1	5.769	5.809	5.769
2	13.765	13.970	13.764
3	21.122	21.569	21.121
4	25.780	26.278	25.734
5	32.319	33.129	32.284

Table 12: Simply supported square isotropic plate with a square hole: Comparison of nondimensionalised natural frequencies between 1D-IRBF and Strand7 results, $\bar{\omega} = \left(\omega b^2/h\right)\sqrt{\rho/E_2}$, $t/b = 0.1$, $K_s = 5/6$.

Mode	IRBF (17×17)	Strand7 (41×41)
1	38.931	38.856
2	39.959	39.805
3	42.503	41.805
4	42.886	44.142
5	46.890	47.964

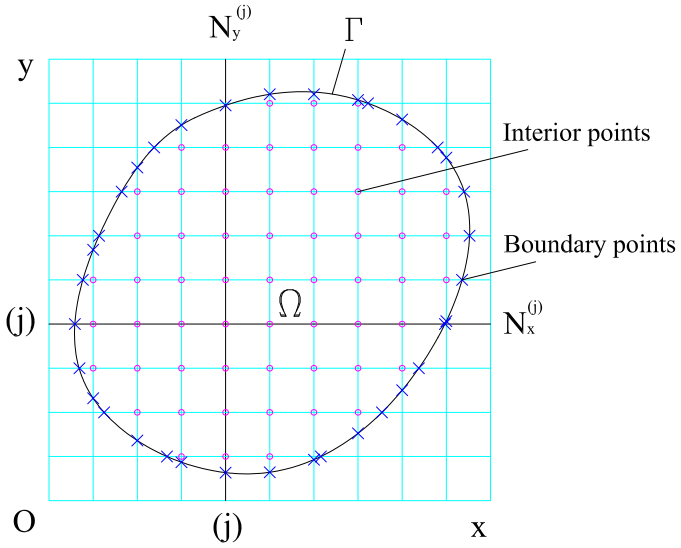

Figure 1: Cartesian grid.

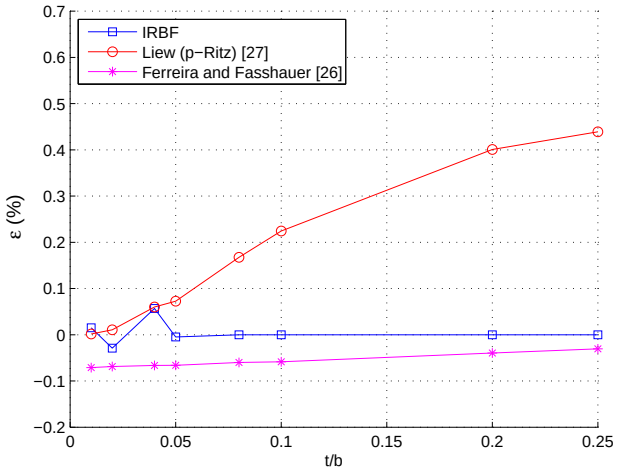

Figure 2: Simply supported four-ply $[0^o/90^o/90^o/0^o]$ square laminated plate: errors of nondimensionalised fundamental frequency ($\epsilon = (\bar{\omega} - \bar{\omega}_E)/\bar{\omega}_E$) with respect to thickness-to-length ratios t/b.

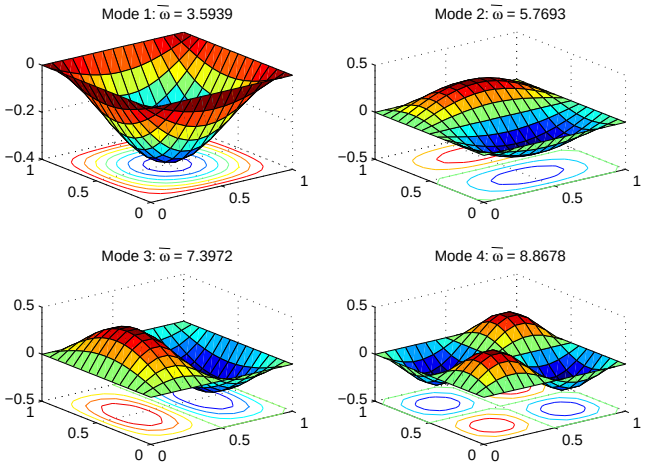

Figure 3: Mode shapes for simply supported three-ply $[0^o/90^o/0^o]$ square laminated plate with $t/b = 0.2$ and grid of 15×15.

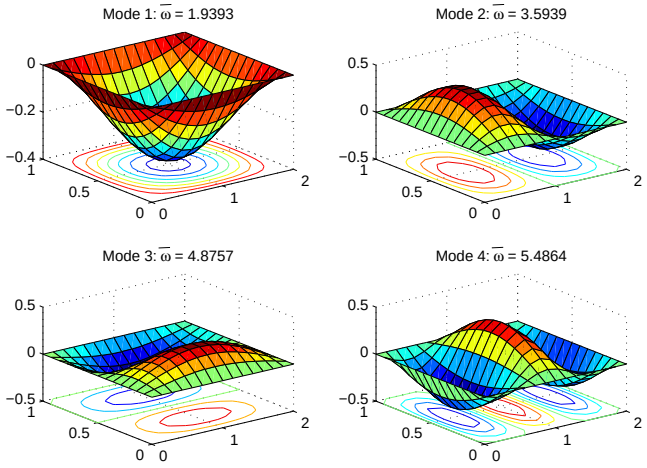

Figure 4: Mode shapes for simply supported three-ply $[0^o/90^o/0^o]$ rectangular laminated plate with $a/b = 2$, $t/b = 0.2$ and grid of 15×15.

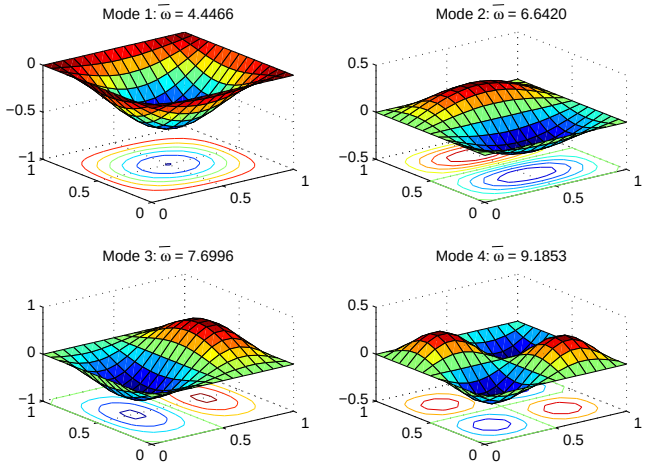

Figure 5: Mode shapes for simply supported three-ply $[0^o/90^o/0^o]$ square laminated plate with $t/b = 0.2$ and grid of 15×15.

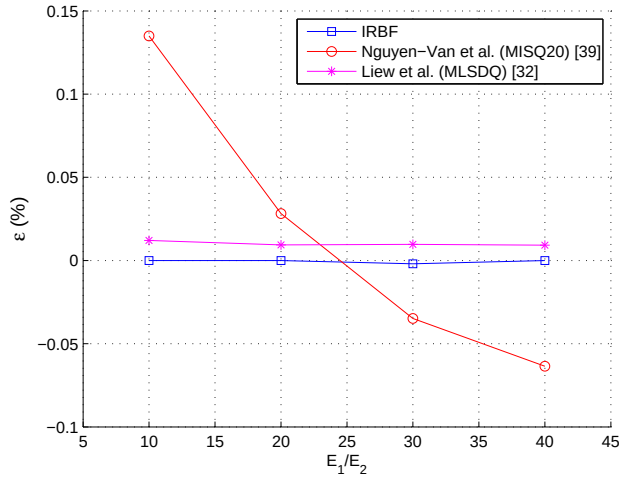

Figure 6: Simply supported four-ply square laminated plate $[0^o/90^o/90^o/0^o]$: errors of nondimensionalised fundamental frequency ($\epsilon = (\bar{\omega} - \bar{\omega}_E)/\bar{\omega}_E$) with respect to modulus ratio E_1/E_2, $t/b = 0.2$.

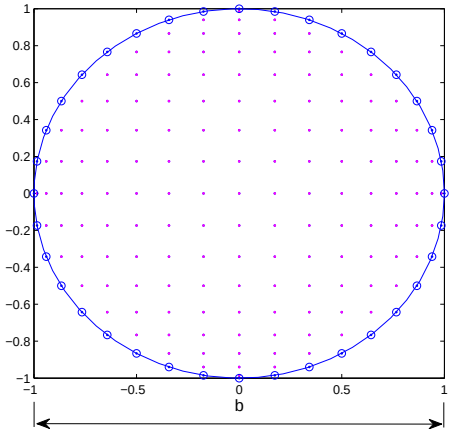

Figure 7: Computational domain of four-ply $[\beta^o/-\beta^o/-\beta^o/\beta^o]$ circular laminated plate.

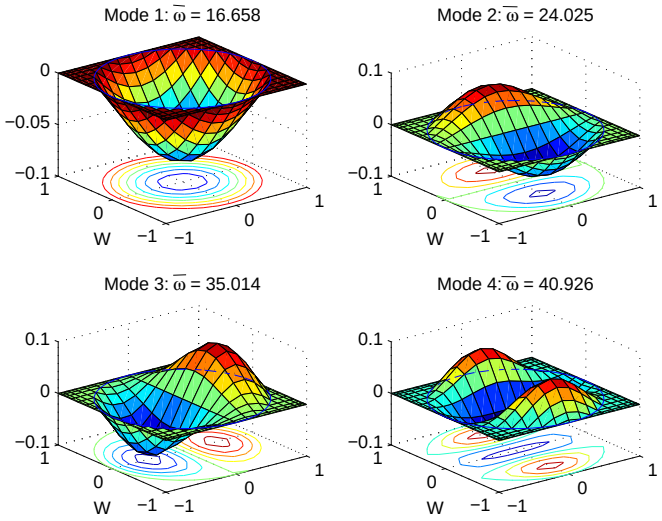

Figure 8: Mode shapes for simply supported four-ply $[45^o/-45^o/-45^o/45^o]$ circular laminated plate, $t/b = 0.1$, grid of 19×19.

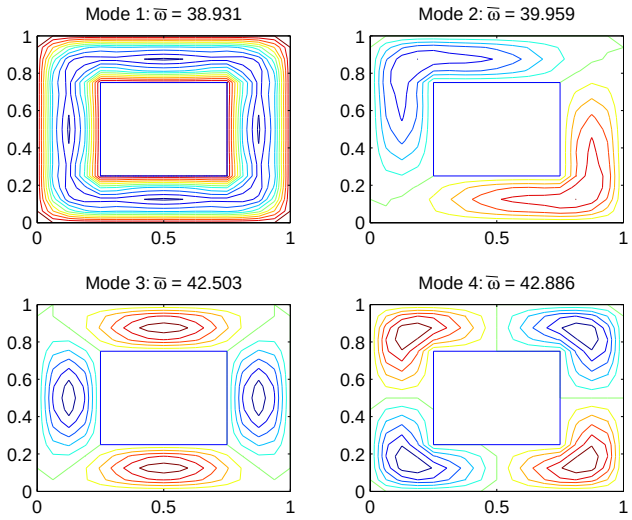

Figure 9: Mode shapes of simply supported square isotropic plate with a square hole, $t/b = 0.1$, grid of 17×17.